



Analytical derivation and analysis of parameter sensitivity for battery electrochemical dynamics

Qingzhi Lai^a, Sidharth Jangra^a, Hyoung Jun Ahn^b, Geumbee Kim^b, Won Tae Joe^b, Xinfan Lin^{a,*}

^a Department of Mechanical and Aerospace Engineering, University of California, Davis, CA, 95616, USA

^b LG Chem Ltd., Seoul, Republic of Korea



HIGHLIGHTS

- Analytic sensitivity expressions of battery electrochemical parameters are derived.
- Features of sensitivity are studied and identified for different parameters.
- The results will enlighten data optimization for parameter estimation.
- The analytic expressions are verified against the simulation based on P2D model.

ARTICLE INFO

Keywords:

Electrochemical battery parameter
Sensitivity analysis
Analytical derivation
Data optimization

ABSTRACT

Model state and parameter estimation is a critical issue in battery research, and it has been recognized that the quality of data plays an important role in determining the accuracy of estimation. Consequently, data optimization for estimation has received increasing attention recently. The key is to evaluate the sensitivity of data to the target variables and design/select the most sensitive data for estimation. However, due to the lack of efficient ways to compute sensitivity and reliance on simulation, data optimization is mostly intractable because of the computational complexity, especially for the first-principle electrochemical battery models. To address this challenge, this paper proposes a methodology to derive the analytic expressions for the sensitivity of battery electrochemical parameters by leveraging reasonable model reformulation, approximation, and simplification techniques. The analytic expressions enable theoretic parameter sensitivity analysis under generic current input, which reveals the fundamental features of the sensitivity and sensitive data for different parameters. The compact expressions also facilitate sensitivity computation for data optimization. The results have been verified by comparing with the exact numerical simulation based on the full order electrochemical model, showing satisfactory fidelity over adequate range of real-world operating conditions.

1. Introduction

State and parameter estimation is an important topic in battery research for various reasons. First, offline system identification is needed to obtain a model with adequate fidelity for model-based analysis, design, simulation, and management of battery performance [1–3]. Second, online estimation of key battery states and parameters, e.g. state of charge (SOC), state of health (SOH), and state of power (SOP), is critical for monitoring and maintaining real-time battery performance in onboard applications [3], such as electric vehicles [2] and unmanned

aerial vehicles (UAV) [4]. The process of estimation involves 3 basic elements, namely the model, algorithm, and data [3]. In general practice, the algorithm fits the model to measurement data, e.g. battery current, voltage, and temperature, to determine the optimal values of the state and parameters. Traditionally, the research in battery estimation is dominated by development of models, including the equivalent circuit model (ECM) [5,6], and first-principle electrochemical models such as the pseudo-2D (P2D) model [1,7], and the simplified single particle model (SPM) [8,9], and design of algorithms, including the Kalman Filter [8,10,11], Moving Horizon Observer [12,13], PDE

* Corresponding author.

E-mail address: lxflin@ucdavis.edu (X. Lin).

Backstepping Observer [14,15], and Lyapunov-based approach among others [16].

The importance of data in estimation, however, has long been neglected. In reality, the sensitivity of the output data to the target variable determines the accuracy of estimation to a large extent. For example, the estimation error variance and bias induced by measurement noises and model uncertainty will be suppressed by sensitive data and amplified by insensitive ones [17–19]. Nevertheless, most existing estimation practice does not take data sensitivity into account. For offline system identification, empirical current excitations are predominantly used, such as the constant-current charging/discharging and pulse current [20,21]. For online estimation, most algorithms simply use all the data points from random online data stream to estimate every target variable. However, it is often the case that the empirical test profiles are only sensitive to a small portion of the model parameters to be identified [22], and only a small fraction of data from the random online data stream are sensitive to the target variables to be estimated in real time [23]. Lack of sensitive data is one of the major causes for inaccurate and unreliable estimation results, which is a fundamental limit imposed by data that cannot be addressed by model or algorithm improvement [17,24].

Research on sensitivity analysis and data optimization for estimation has been receiving increasing attention recently [3]. Some early works numerically computed the sensitivity of battery states and parameters to existing test data, and determined the variables that are robustly identifiable [22,25,26]. Some later ones focused on designing current excitation to optimize the sensitivity or sensitivity-related metrics, e.g. Fisher information matrix and Cramer-Rao bound, for the model parameters to be estimated [27–30]. More recently, the work in Refs. [23] proposed a data selection/mining strategy for real-time estimation, which aims at identifying and using sensitive data points/segments from random online stream for estimation. These works have demonstrated promising results in guaranteeing and improving the quality of battery state and parameter estimation.

Despite these significant progress, major challenges still remain to be addressed. So far, most results regarding data optimization for estimation are limited to the equivalent circuit model, which is a phenomenological model capturing battery macroscopic dynamics. The new trend in battery control and estimation is to use the first-principle electrochemical models, e.g. P2D and SPM [1,8,9], due to their high fidelity and capability of capturing battery physical dynamics. For these models, however, most existing studies are limited to numerical sensitivity analysis and sensitive variable screening under specific data sets [22,25], and there is not much progress in sensitivity analysis for generic data and data optimization for estimation. Recently, the work of [30] made an important contribution in formulating an optimal experiment design problem, where miscellaneous current profiles, including pulses, sine waves, and drive cycles, are chosen from a pre-determined library to maximize the Fisher information of the parameters of a P2D model. Nevertheless, the result is only optimal within the empirically determined input library but not necessarily the ultimate optimal current profile. It is of great interest to find the ultimate optimal profile not subject to any pre-set pattern, and explore the fundamental signatures/features of the optimal data for estimating different parameters. The main obstacle facing data optimization for electrochemical model-based estimation is the complexity of sensitivity calculation. The exact approach is to solve the sensitivity differential equations (SDEs), which are obtained by taking the partial derivative of the original model equations to the target variables [25,30]. Due to lack of analytic solution under generic input, SDEs are typically solved through numerical simulation together with the original model equations. The associated computational load is intractable for optimization, since most algorithms need to solve the equations iteratively over a large search space to find the optimum [30]. The computational complexity also poses great challenge to data selection/mining for real-time estimation, which is subject to stringent constraint on computational power, memory, and

time.

The goal of this paper is to derive the analytic expressions for the sensitivity of battery electrochemical parameters based on reasonable model simplification, approximation and reduction techniques. The analytical expression is the key to enable theoretic sensitivity analysis under generic current input, tractable offline optimization, and efficient online computation. The contributions of the paper include the following three aspects. First, we formulate a methodology for deriving the sensitivity of generic P2D model parameters. It will be shown that for most electrochemical parameters, their sensitivity is composed by a non-dynamic component, which is mainly related to the instantaneous input current, and a semi-linear dynamic component, which also depends on the history of current [31]. To capture the dynamics of sensitivity, we propose to derive a transfer function from current input to the sensitivity, i.e. the sensitivity transfer function (STF). This frequency-domain approach is inspired by our previous work on the battery equivalent circuit model [24], and leverages the single particle assumption, Laplace transform, and Padé approximation. The method is applied to derive the sensitivity for several critical parameters including the solid and electrolyte phase lithium diffusion coefficient D_s and D_e , volume fraction of the electrode active material ε_s , electrode porosity ε_e , separator porosity ε_{sep} , and reaction rate constant k . Second, in-depth understanding on the features of parameter sensitivity and sensitive data is obtained from the derived expressions. For example, the STFs are used to analyze the frequency spectrum of dynamic sensitivity and the bandwidth of sensitive data for different parameters, which provide useful insights on data (input) optimization/selection for estimating these parameters. Third, the derived sensitivity based on SPM is compared with the exact numerical computation based on the P2D model for verification. It is shown that the SPM-based sensitivity matches reasonably well with that of the P2D model within adequate range of operating conditions, demonstrating the validity of the derived analytic expressions.

2. Pseudo-2D electrochemical battery model and single particle simplification

The electrochemical battery model under investigation, namely the Pseudo-2D (P2D) electrochemical model, is based on the theory of porous electrode and concentrated solution [1]. The model provides a microscopic description of lithium diffusion and electrochemical reaction kinetics inside the battery, and establishes the relationship between internal states, external current input, and voltage output. Due to the computational complexity of solving the coupled partial differential equations (PDEs) in the P2D model, extensive research has been devoted to exploring model reduction/simplification. The single particle model with electrolyte dynamics (SPMe) is a popular simplification, especially for real-time control applications. The SPMe is derived under the assumption of uniform reaction current density across the battery electrode, so that a single particle can be used to represent the whole electrode, as shown in Fig. 1. The model is capable of capturing the electrochemical processes occurring in the anode, separator and cathode regions including the diffusion of lithium ions in the active material and the electrolyte, and the intercalation/deintercalation of lithium ion into/from the electrode particle. The explicit structure of SPMe makes it feasible to derive the analytic sensitivity of the battery electrochemical parameters, which is the objective of this paper. In this section, a brief overview of the P2D and SPMe models is presented.

2.1. Solid-phase lithium diffusion

Based on the Fick's second law, the dynamics of lithium diffusion in an electrode particle is described in spherical coordinate by Eqn. (1), with the boundary conditions given in Eqn. (2) and Eqn. (3). The equation predicts how diffusion causes the solid-phase lithium concentration c_s to change under external input over time along the radius direction of a particle. The subscript i denotes the positive electrode

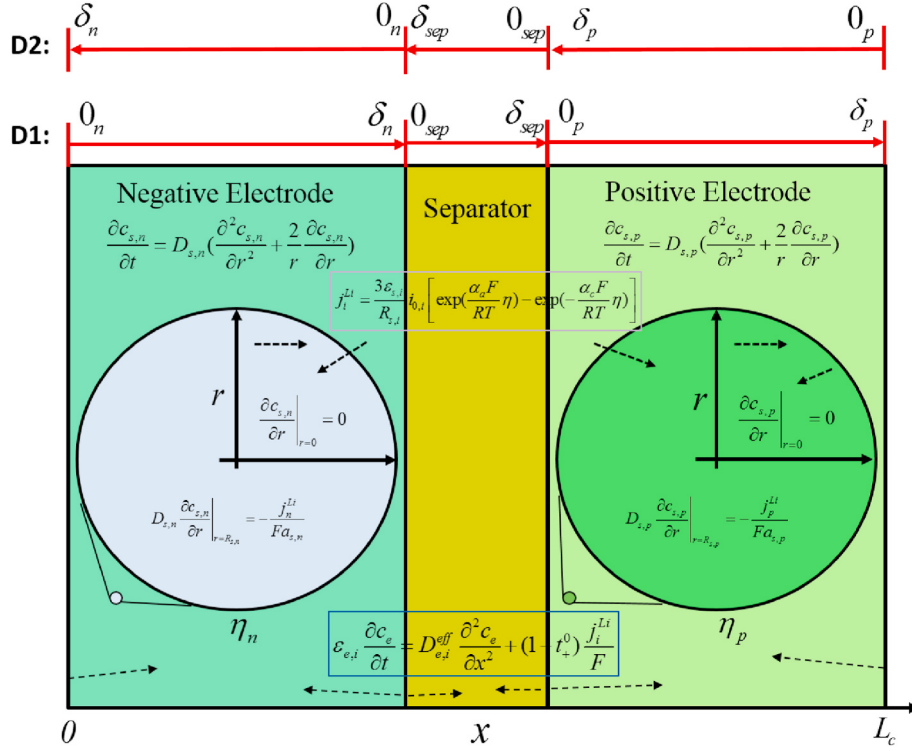


Fig. 1. Schematic of single particle model with electrolyte dynamics.

(cathode) when $i = p$ or negative electrode (anode) when $i = n$.

$$\frac{\partial c_{s,i}}{\partial t} = D_{s,i} \left(\frac{\partial^2 c_{s,i}}{\partial r^2} + \frac{2}{r} \frac{\partial c_{s,i}}{\partial r} \right) \quad (1)$$

$$\frac{\partial c_{s,i}}{\partial r} \Big|_{r=0} = 0 \quad (2)$$

$$D_{s,i} \frac{\partial c_{s,i}}{\partial r} \Big|_{r=R_{s,i}} = - \frac{j_i^{Li}}{a_{s,i} F} \quad (3)$$

In the equations, D_s is the solid-phase diffusion coefficient, r is the radial coordinate, R_s is the electrode particle radius, a_s is the specific interfacial area ($a_s = \frac{3\epsilon_s}{R_s}$), ϵ_s is the active material volume fraction, F is the Faraday constant, and j_i^{Li} is the intercalation/deintercalation current density. The sign for deintercalation current is positive while that for intercalation current is negative. Under the single particle assumption, j_i^{Li} is assumed to be uniform along the electrode thickness (x) direction, and can be computed as the average current over the electrode thickness,

$$j_i^{Li} = \pm \frac{I}{A\delta_i}, \quad (4)$$

where I is the current, A is the electrode area, and δ is the thickness of the region.

Padé approximation is used in this paper to simplify the PDE by deriving a transfer function from I to the lithium concentration at the particle surface c_{se} [32]. First, Laplace transform is applied to convert Eqn. (1) to an ODE of c_s with respect to the radial coordinate r in the frequency domain, yielding

$$D_{s,i} \frac{d^2 C_{s,i}(s)}{dr^2} + \frac{2D_{s,i}}{r} \frac{dC_{s,i}(s)}{dr} - sC_{s,i}(s) = 0 \quad (5)$$

Then by solving Eqn. (5) at the particle surface ($r = R_s$) under the specified boundary conditions, a transcendental transfer function for surface concentration c_{se} is obtained as

$$\frac{C_{se,i}(s)}{I} = - \frac{\left(e^{2R_{s,i}\sqrt{\frac{s}{D_{s,i}}}} - 1 \right) \frac{R_{s,i}^2}{3A\delta_i F \epsilon_{s,i} D_{s,i}}}{1 + R_{s,i}\sqrt{\frac{s}{D_{s,i}}} + e^{2R_{s,i}\sqrt{\frac{s}{D_{s,i}}}} \left(R_{s,i}\sqrt{\frac{s}{D_{s,i}}} - 1 \right)} \quad (6)$$

Finally, Padé approximation is applied to simplify the transcendental transfer function to a rational transfer function, of which the coefficients are determined by moment matching [32]. In this paper, a 3rd order Padé approximation is adopted,

$$C_{se,i}(s) \approx - \left[\frac{7R_{s,i}^4 s^2 + 420D_{s,i}R_{s,i}^2 s + 3465D_{s,i}^2}{F\epsilon_{s,i}s(R_{s,i}^4 s^2 + 189D_{s,i}R_{s,i}^2 s + 3465D_{s,i}^2)} \right] \frac{I(s)}{A\delta_i}, \quad (7)$$

which matches up to 3rd order moment of Eqn. (6). The surface concentration c_{se} affects the battery terminal voltage through the open circuit potential, $U(c_{se})$, which is typically a nonlinear function of c_{se} depending on the battery chemistry.

For real-time application, the rational transfer function in Eqn. (7) can be implemented in time domain through the state space representation to compute the evolution of c_{se} over time driven by input current I . We will use Eqn. (7) in subsequent sections to derive the sensitivity transfer function of D_s and ϵ_s .

2.2. Liquid-phase lithium diffusion

Electrolyte is the medium in which the lithium ions migrate between the cathode and the anode through the separator. The lithium ion concentrations in the electrolyte, c_e , of the three regions are governed by two physical processes, namely the diffusion caused by the concentration gradient, and the generation or consumption of lithium ion flow (current) j_i^{Li} by the intercalation/deintercalation reaction (except in the separator). Therefore, the dynamics can be described by the Fick's second law in Cartesian coordinate defined by 'D1' in Fig. 1 plus a source

term featuring j_i^{Li} ,

$$\begin{aligned} \text{Anode : } & \varepsilon_{e,n} \frac{\partial c_e}{\partial t} = D_{e,n}^{\text{eff}} \frac{\partial^2 c_e}{\partial x^2} + (1 - t_+^0) \frac{j_n^{Li}}{F}, \quad (0 \leq x \leq \delta_n) \\ \text{Separator : } & \varepsilon_{e,sep} \frac{\partial c_e}{\partial t} = D_{e,sep}^{\text{eff}} \frac{\partial^2 c_e}{\partial x^2}, \quad (\delta_n < x \leq \delta_n + \delta_{sep}) \\ \text{Cathode : } & \varepsilon_{e,p} \frac{\partial c_e}{\partial t} = D_{e,p}^{\text{eff}} \frac{\partial^2 c_e}{\partial x^2} + (1 - t_+^0) \frac{j_p^{Li}}{F}, \quad (\delta_n + \delta_{sep} < x \leq L_c) \end{aligned} \quad (8)$$

with boundary conditions

$$\begin{aligned} c_e|_{x=\delta_n^-} &= c_e|_{x=\delta_n^+}, \quad c_e|_{x=(\delta_n+\delta_{sep})^-} = c_e|_{x=(\delta_n+\delta_{sep})^+}, \\ D_{e,n}^{\text{eff}} \frac{\partial c_e}{\partial x}|_{x=0} &= 0, \quad D_{e,p}^{\text{eff}} \frac{\partial c_e}{\partial x}|_{x=L_c} = 0, \\ D_{e,n}^{\text{eff}} \frac{\partial c_e}{\partial x}|_{x=\delta_n^-} &= D_{e,sep}^{\text{eff}} \frac{\partial c_e}{\partial x}|_{x=\delta_n^+}, \\ D_{e,sep}^{\text{eff}} \frac{\partial c_e}{\partial x}|_{x=(\delta_n+\delta_{sep})^-} &= D_{e,p}^{\text{eff}} \frac{\partial c_e}{\partial x}|_{x=(\delta_n+\delta_{sep})^+}, \end{aligned} \quad (9)$$

where ε_e is the porosity, D_e^{eff} is the effective diffusion coefficient of electrolyte ($D_e^{\text{eff}} = D_e \varepsilon_e^{1.5}$), D_e is the electrolyte diffusion coefficient, t_+^0 is the transference number, and L_c is the total thickness of the three regions in battery ($L_c = \delta_n + \delta_{sep} + \delta_p$). The subscript *sep* denotes the separator region, and the superscripts '-' and '+' of δ stands for the left and right boundary of the interface respectively. Similar to the solid-phase lithium diffusion, single particle assumption and Padé approximation can be used to derive the transfer function from current to the lithium concentration in the electrolyte c_e . By applying Laplace transform to Eqn. (8) and solving for $c_e(x, s)$ under the uniform j_i^{Li} assumption in Eqn. (4), following transcendental transfer functions can be obtained for the three regions respectively,

$$\begin{aligned} C_{e,n}(s) &= C_1 e^{\sqrt{\frac{s}{D_{e,n}^{\text{eff}}}} x} + C_2 e^{-\sqrt{\frac{s}{D_{e,n}^{\text{eff}}}} x} + \frac{(1 - t_+^0) I(s)}{A \delta_n F \mathcal{E}_{e,n} s} \\ C_{e,sep}(s) &= C_3 e^{\sqrt{\frac{s}{D_{e,sep}^{\text{eff}}}} x} + C_4 e^{-\sqrt{\frac{s}{D_{e,sep}^{\text{eff}}}} x} \\ C_{e,p}(s) &= C_5 e^{\sqrt{\frac{s}{D_{e,p}^{\text{eff}}}} x} + C_6 e^{-\sqrt{\frac{s}{D_{e,p}^{\text{eff}}}} x} - \frac{(1 - t_+^0) I(s)}{A \delta_p F \mathcal{E}_{e,p} s} \end{aligned} \quad (10)$$

The coefficients C_1, C_2, C_3, C_4, C_5 and C_6 can be obtained by matching the 6 boundary conditions in Eqn. (9). Of particular interest are the transfer functions evaluated at the two terminals, namely $x = 0_n$ and $x = \delta_p$ under the coordinate defined by 'D1' as shown in Fig. 1, which will be subsequently used for determining the battery terminal voltage. Padé approximation is then applied to simplify the transcendental transfer functions to low order rational ones. In this paper, the 1st order Padé approximation is adopted since it is sufficient to match the original transcendental transfer function over a wide frequency range as shown later. During the derivation, the same porosity ε_e value is assumed for the cathode and anode regions with a different one for the separator $\varepsilon_{e,sep}$, which is valid for most lithium ion batteries according to literature [8,30]. Compared with most prior works which assumed same ε_e in all 3 regions [9], the assumption in this paper is more generic and reasonable but significantly complicates the Padé approximation process and the expression of the resultant coefficients. It is found that the complexity of the coefficient expressions depends on how the direction of the x coordinates is defined. Under the coordinate defined by 'D1' in Fig. 1, a simpler form of the Padé-approximated transfer function can be obtained at $x = \delta_p$, but that at $x = 0_n$ is overwhelmingly complicated. On the other hand, by defining the x -direction in a symmetric but opposite way as shown by 'D2' in Fig. 1, a simple transfer function can be obtained at $x = \delta_n$ with a complicated one at $x = 0_p$. Therefore, the

best approach is to employ these two different coordinate definitions to derive the two transfer functions respectively. In addition, due to the difficulty of deriving the Padé-approximated transfer function by keeping the electrode and separator thickness, namely δ_p , δ_n and δ_{sep} , as generic symbols, we applied their numerical values during derivation for simplicity. For example, by taking $\delta_p = 10 \times 10^{-5} m$, $\delta_n = 10 \times 10^{-5} m$, and $\delta_{sep} = 2.5 \times 10^{-5} m$ as in Ref. [33], the obtained 1st order transfer function for the electrolyte lithium concentration at the electrode boundaries is

$$C_{e,i}(s) \approx (\pm) \frac{\frac{\varepsilon_e^{1.5} + 4\varepsilon_{e,sep}^{1.5}}{8 \times 10^4 D_e \varepsilon_e^{1.5} \varepsilon_{e,sep}^{1.5}} \frac{(1 - t_+^0)}{AF}}{1 + \frac{1.92 \times 10^{10}}{(4D_e \varepsilon_e^{0.5} \varepsilon_{e,sep}^3 + D_e \varepsilon_e^{2.5} \varepsilon_{e,sep}^1)} \cdot s} \cdot I(s), \quad (11)$$

which applies to both cathode (at $x = 0_n$ in 'D1' in Fig. 1) and anode (at $x = \delta_p$ in 'D1' in Fig. 1) since both the porosity and thickness of the two electrodes are identical under the given parameter set.

The electrolyte potential φ_e can be obtained based on the Ohm's law and the electrical effect of the lithium ion concentration variation as [1, 7].

$$i_e = -\kappa^{\text{eff}} \frac{\partial \varphi_e}{\partial x} + \frac{2\kappa^{\text{eff}} RT (1 - t_+^0)}{F} (1 + \gamma) \frac{\partial \ln c_e}{\partial x} \quad (12)$$

$$\frac{\partial i_e}{\partial x} = j_i^{Li} \quad (13)$$

where i_e is the current flow in the electrolyte, κ^{eff} is the effective electrolyte conductivity ($\kappa^{\text{eff}} = \kappa \varepsilon_e^{1.5}$), κ is the conductivity of electrolyte, R is the universal gas constant, T is the temperature, and γ is the activity coefficient. The current flow i_e can be easily obtained by integrating the constant j_i^{Li} over x as in Eqn. (13). Then by solving Eqn. (12) j_i^{Li} the electrolyte potential difference between the two terminals can be computed as

$$\Delta \varphi_e = \varphi_e(L_c) - \varphi_e(0) = \varphi_{e,p} - \varphi_{e,n} = \Delta \varphi_{e,con} - \Delta \varphi_{e,\Omega}, \quad (14)$$

which includes a lithium concentration polarization term,

$$\Delta \varphi_{e,con} = \frac{2RT(1 - t_+^0)}{F} (1 + \gamma) \ln \left(\frac{c_{e,p}}{c_{e,n}} \right) \quad (15)$$

and an Ohmic polarization term,

$$\begin{aligned} \Delta \varphi_{e,\Omega} &= \int_{0^-}^{\delta_n} \frac{I}{A \kappa_{e,n}^{\text{eff}} \delta_n} dx + \int_{0^+}^{\delta_{sep}} \frac{I}{A \kappa_{sep}^{\text{eff}}} dx + \int_{0^+}^{\delta_p} \frac{I}{A \kappa_p^{\text{eff}} \delta_p} dx \\ &= \frac{I(\delta_p + \delta_n)}{2A \kappa_e^{1.5}} + \frac{I \delta_{sep}}{A \kappa_{e,sep}^{1.5}} \end{aligned} \quad (16)$$

In Eqn. (15), $c_{e,p}$ and $c_{e,n}$ can be calculated by using the time domain state space representation of the transfer function in Eqn. (11).

We will subsequently use Eqns. (11), (15) and (16) to analytically derive the sensitivity of the electrolyte lithium diffusion coefficient D_e , porosity ε_e and $\varepsilon_{e,sep}$.

2.3. Lithium intercalation/deintercalation

The lithium intercalation/deintercalation reaction at the electrode particle surface, i.e. the insertion/removal of lithium ions into/from the particle, is driven by the overpotential

$$\eta_i = \varphi_{s,i} - \varphi_{e,i} - U_i(c_{se,i}) - R_{f,i} \frac{j_i^{Li}}{a_{s,i}}, \quad (17)$$

which is the surplus of the electrode potential φ_s over the electrolyte potential φ_e , open circuit potential U that depends on the surface concentration c_{se} , and the Ohmic potential drop over the solid-electrolyte-

interphase (SEI) film resistance R_f . The overpotential governs the reaction current density j_i^{Li} based on the Butler-Volmer Equation,

$$j_i^{Li} = a_{s,i} i_{0,i} \left[\exp\left(\frac{\alpha_a F}{RT} \eta_i\right) - \exp\left(-\frac{\alpha_c F}{RT} \eta_i\right) \right], \quad (18)$$

where α_a and α_c are the anodic and cathodic charge transfer coefficients respectively. The exchange current $i_{0,i}$ takes the form

$$i_{0,i} = F k_i (c_e)^{\alpha_a} \left(c_{se,i}^{\max} - c_{se,i} \right)^{\alpha_a} (c_{se,i})^{\alpha_c}, \quad (19)$$

with k being the reaction rate constant, c_s^{\max} being the maximum concentration of the solid material.

In SPMe, since j_i^{Li} has been obtained based on the single particle assumption in Eqn. (4) and it is assumed that $\alpha_a = \alpha_c$, the overpotential η_i can be calculated by inverting Eqn. (18) as

$$\eta_i = \frac{RT}{\alpha_a F} \ln \left(\xi_i + \sqrt{\xi_i^2 + 1} \right), \quad (20)$$

where

$$\xi_i = \frac{j_i^{Li}}{2a_{s,i} i_{0,i}} \quad (21)$$

We will subsequently use Eqn. (20) and Eqn. (21) to analytically derive the sensitivity for ϵ_s and k .

2.4. Battery terminal voltage

The measurable output of the model, i.e. battery terminal voltage, is the solid-phase potential difference between the boundaries of the cathode and anode plus the voltage drop over a resistance R_c , which includes the resistance of current collectors and all wiring,

$$V = \varphi_s(L_c) - \varphi_s(0) - R_c \frac{I}{A} = \varphi_{s,p} - \varphi_{s,n} - R_c \frac{I}{A} \quad (22)$$

According to Eqn. (17), $\varphi_{s,i}$ can be calculated as

$$\varphi_{s,i} = \eta_i + \varphi_{e,i} + U_i(c_{se,i}) + R_{f,i} \frac{j_i^{Li}}{a_{s,i}} \quad (23)$$

Therefore, by combining Eqn. (22) and Eqn. (23) the battery terminal voltage is obtained as,

$$V = \varphi_{s,p} - \varphi_{s,n} = (U_p - U_n) + (\varphi_{e,p} - \varphi_{e,n}) + (\eta_p - \eta_n) - \left(R_c \frac{I}{A} + \frac{IR_{f,p}}{A\delta_p a_{s,p}} + \frac{IR_{f,n}}{A\delta_n a_{s,n}} \right) \quad (24)$$

By lumping all Ohmic resistance into R_Ω , and decomposing $\varphi_{e,p} - \varphi_{e,n}$ to $\Delta\varphi_{e,con}$ and $\Delta\varphi_{e,ohm}$ according to Eqn. (14), Eqn. (24) can be rewritten as

$$V = U_p(c_{se,p}) - U_n(c_{se,n}) + \Delta\varphi_{e,con}(c_e) + \eta_p(c_{se,p}) - \eta_n(c_{se,n}) - IR_\Omega, \quad (25)$$

where

$$R_\Omega = \frac{R_c}{A} + \frac{R_{f,p}}{A\delta_p a_{s,p}} + \frac{R_{f,n}}{A\delta_n a_{s,n}} + \frac{\delta_p + \delta_n}{2A\kappa\epsilon_e^{1.5}} + \frac{\delta_{sep}}{A\kappa\epsilon_{sep}^{1.5}} \quad (26)$$

In Eqn. (25), c_{se} , $\Delta\varphi_{e,con}$, and η have been obtained in the previous sub-models. It is seen that the terminal voltage can be decomposed into 4 parts, which are related to the open circuit potential U , electrolyte concentration polarization potential $\Delta\varphi_{e,con}$, overpotential η , and lumped ohmic resistance R_Ω respectively.

3. Methodology and procedures for deriving parameter sensitivity

The (voltage) sensitivity of a generic battery parameter θ , $\frac{\partial V}{\partial \theta}$, can be obtained by applying the chain rule of differentiation to the voltage

equation in Eqn. (25),

$$\begin{aligned} \frac{\partial V}{\partial \theta} &= \frac{\partial U(c_{se})}{\partial \theta} + \frac{\partial \Delta\varphi_{e,con}(c_e)}{\partial \theta} + \frac{\partial \eta(c_{se}, a_s)}{\partial \theta} - \frac{\partial R_\Omega}{\partial \theta} I \\ &= \frac{\partial U(c_{se})}{\partial c_{se}} \frac{\partial c_{se}}{\partial \theta} + \frac{\partial \Delta\varphi_{e,con}(c_e)}{\partial c_e} \frac{\partial c_e}{\partial \theta} + \left(\frac{\partial \eta}{\partial c_{se}} \frac{\partial c_{se}}{\partial \theta} + \frac{\partial \eta}{\partial a_s} \frac{\partial a_s}{\partial \theta} \right) - \frac{\partial R_\Omega}{\partial \theta} I \end{aligned} \quad (27)$$

Among all the terms in Eqn. (27), $\frac{\partial R_\Omega}{\partial \theta} I$ is referred to as the linear non-dynamic term as it is related to the linear ohmic resistance R_Ω and not subject to system dynamics, e.g. lithium ion diffusion; $\frac{\partial \eta}{\partial a_s} \frac{\partial a_s}{\partial \theta}$ is the nonlinear non-dynamic term as it is related to the nonlinear overpotential η and not subject to system dynamics; $\frac{\partial U(c_{se})}{\partial c_{se}} \frac{\partial c_{se}}{\partial \theta}$, $\frac{\partial \Delta\varphi_{e,con}(c_e)}{\partial c_e} \frac{\partial c_e}{\partial \theta}$ and $\frac{\partial \eta}{\partial c_{se}} \frac{\partial c_{se}}{\partial \theta}$ are the semi-linear dynamic terms, as they depend on both the sensitivity of certain states, i.e. $\frac{\partial c_{se}}{\partial \theta}$ or $\frac{\partial c_e}{\partial \theta}$, which are governed by the linear diffusion dynamics, and a certain nonlinear coefficient, i.e. $\frac{\partial U(c_{se})}{\partial c_{se}}$, $\frac{\partial \Delta\varphi_{e,con}(c_e)}{\partial c_e}$ or $\frac{\partial \eta}{\partial c_{se}}$.

Different procedures need to be applied to derive the dynamic and non-dynamic terms of sensitivity, as summarized in the flowchart shown in Fig. 2. The derivation of non-dynamic terms is straightforward, which only involves taking the partial derivative to θ to obtain the sensitivity as a function of the input current. The derivation of dynamic terms is more complicated since the state sensitivity, $\frac{\partial c_{se}}{\partial \theta}$ and $\frac{\partial c_e}{\partial \theta}$, depends on the diffusion dynamics of c_{se} or c_e and will evolve over time even under constant input current. To characterize the dynamics of the state sensitivity in an analytic and compact manner, we apply frequency-domain techniques to derive a transfer function from input current I to the state sensitivity, which is referred to as the sensitivity transfer function (STF). Specifically, by performing the Laplace transform, the linear governing PDE of the state dynamics is converted to a frequency domain ODE. The ODE is then solved along with the boundary conditions to obtain a transfer function from current to the state, which is typically transcendental. Padé approximation is then used to simplify the transcendental transfer function to a low order rational transfer function to facilitate the derivation of sensitivity and implementation in time domain. The above steps have already been performed in Section 2. It is noted that the obtained transfer function is analytical as the coefficients are explicitly dependent on the physical parameter θ . Therefore, by taking the partial derivative of the transfer function to θ , the STF from current I to $\frac{\partial c}{\partial \theta}$ is obtained. The STF can be converted to time domain, e.g. via state space representation, to compute the evolution of the state sensitivity over time conveniently, which can then be multiplied by the nonlinear coefficient to calculate the dynamic terms of the voltage sensitivity. Finally, the (total) voltage sensitivity can be obtained by combining the dynamic terms and the non-dynamic terms.

4. Derivation of sensitivity for specific parameters

In this section, the formulated methodology is applied to derive the sensitivity of specific battery electrochemical parameters, including the solid phase diffusion coefficient D_s , the volume fraction of the electrode active material ϵ_s , the reaction rate constant k , porosity ϵ_e and ϵ_{sep} , and electrolyte diffusion coefficient D_e . These parameters have major impacts on battery electrochemical behaviors and key performance indexes including SOC, SOH, and SOP. The proposed methodology can be applied to other parameters without loss of generality.

4.1. Sensitivity of solid phase diffusion coefficient D_s

The solid phase diffusion coefficient D_s affects the particle surface lithium concentration c_{se} and hence the battery terminal voltage V through the open circuit potential U and overpotential η , according to Eqn. (7) and Eqn. (25). Therefore, by applying the chain rule of differentiation, the sensitivity of D_s can be obtained as

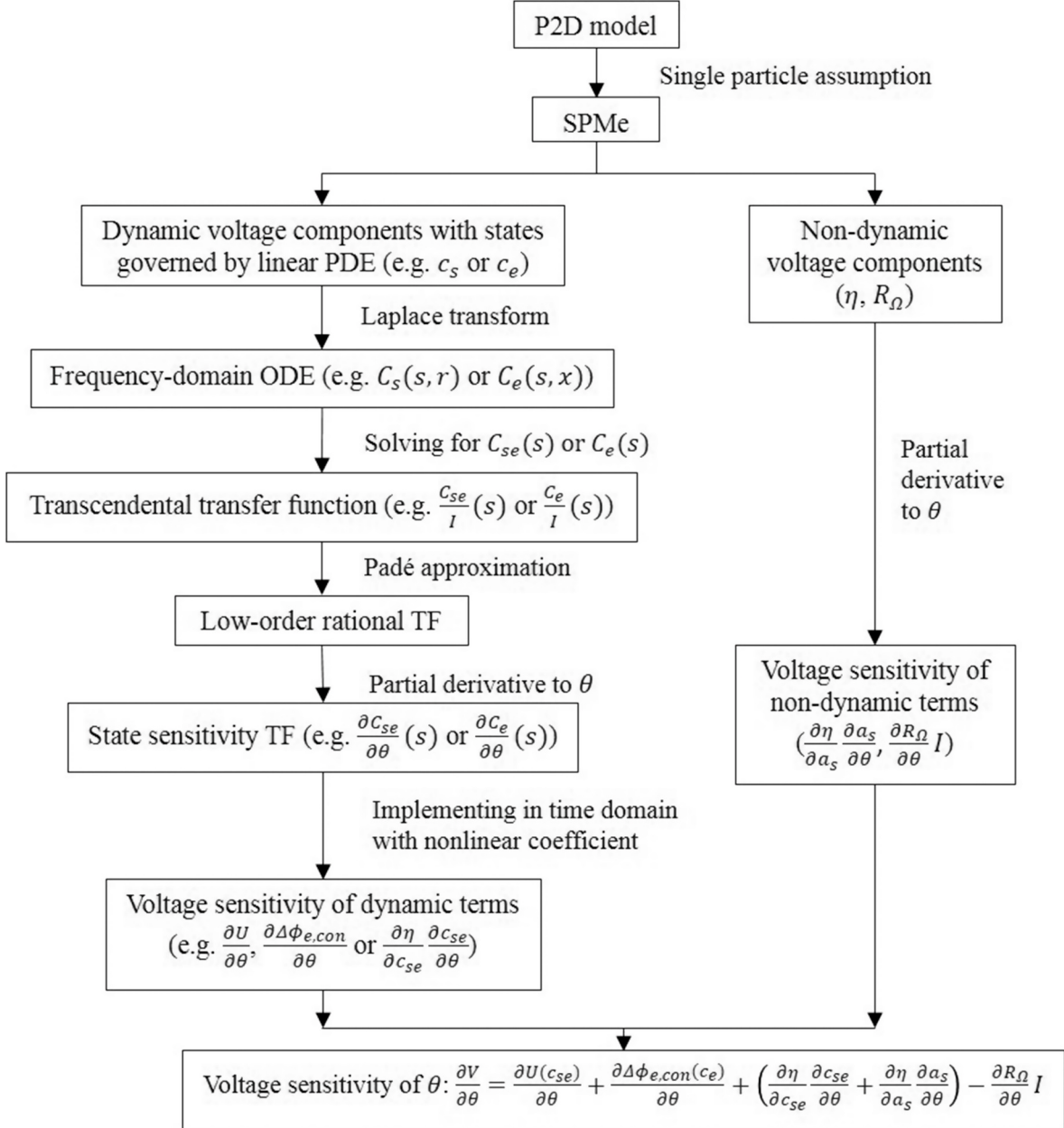


Fig. 2. Flowchart of parameter sensitivity derivation.

$$\frac{\partial V}{\partial D_s} = \left(\frac{\partial U}{\partial c_{se}} + \frac{\partial \eta}{\partial c_{se}} \right) \cdot \frac{\partial c_{se}}{\partial D_s}, \quad (28)$$

where $\frac{\partial U}{\partial c_{se}}$ is the slope of the open circuit potential (OCP). The second term, $\frac{\partial \eta}{\partial c_{se}} \frac{\partial c_{se}}{\partial D_s}$, represents the impact of D_s on the exchange current i_0 which affects the overpotential through the particle surface concentration c_{se} , where $\frac{\partial \eta}{\partial c_{se}}$ can be obtained as

$$\frac{\partial \eta}{\partial c_{se}} = \frac{RT}{2a_a F} \frac{1}{\sqrt{1 + \xi^2}} [c_e c_{se} c_s^{max} - c_{se}]^{-1} (c_e c_s^{max} - 2c_e c_{se}) \quad (29)$$

The key step then is to derive the expression for $\frac{\partial c_{se}}{\partial D_s}$. Since lithium diffusion is a dynamic process, the impact of D_s on c_{se} will change over time and needs to be captured with a dynamic model. This can be achieved by using the analytical transfer function from I to c_{se} obtained in Eqn. (7). By taking the partial derivative of Eqn. (7) to D_s , a sensitivity transfer function (STF) for $\frac{\partial c_{se}}{\partial D_s}$ can be obtained as

$$\frac{\partial c_{se}}{\partial D_s}(s) = \frac{21R_s^2(43R_s^4s^2 + 1980D_sR_s^2s + 38115D_s^2)}{F\varepsilon_s A \delta(R_s^4s^2 + 189D_sR_s^2s + 3465D_s^2)^2} I(s) \quad (30)$$

The coefficients in Eqn. (30) are in the form of symbolic battery parameters, which are easily adaptable to different battery chemistries. The derived STF can be conveniently used for both frequency domain and time domain analysis.

In frequency domain, the dynamic nature of $\frac{\partial c_{se}}{\partial D_s}$ can be studied based on the Bode plot of the sensitivity transfer function. Fig. 3a shows the Bode plot of the normalized sensitivity $\frac{\partial c_{se}}{\partial D_s} D_s$ for the cathode of the battery using parameter values in Ref. [33]. The blue solid line represents the frequency response of the analytic STF, and the red line shows that of the sensitivity obtained based on the transcendental transfer function in Eqn. (6). The two matches very well at low frequency (up to around 0.1 Hz), since the moment matching to determine the Padé approximation coefficients is performed at $s = 0$. The fidelity is

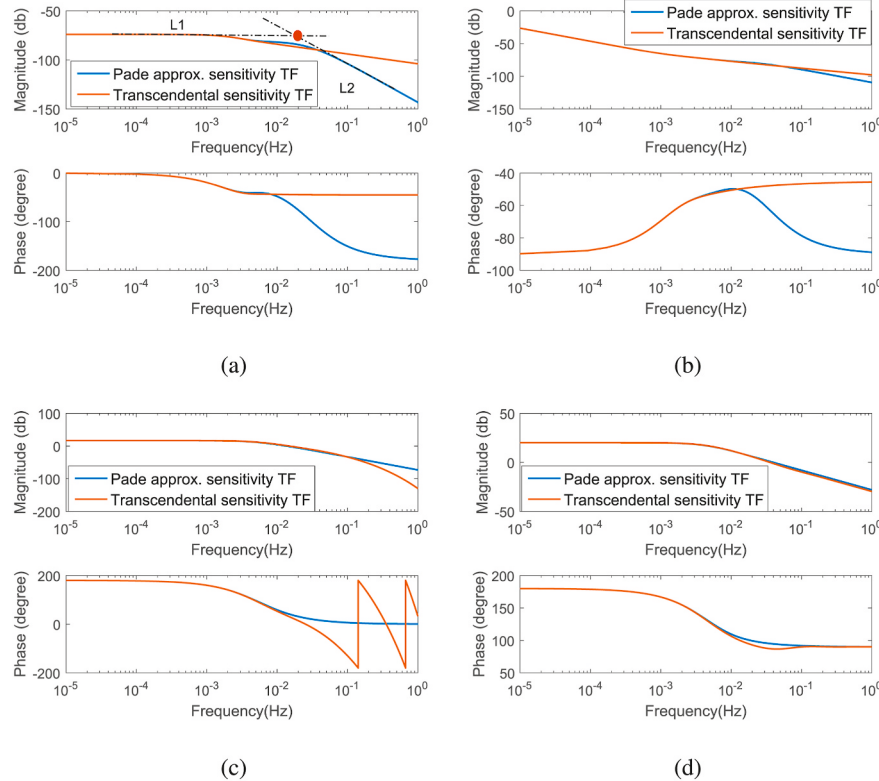


Fig. 3. (a) Bode plot of normalized sensitivity transfer function for $\frac{\partial C_{se,p}}{\partial D_s}$; (b) Bode plot of normalized sensitivity transfer function for $\frac{\partial C_{se,p}}{\partial D_s^2}$; (c) Bode plot of normalized sensitivity transfer function for $\frac{\partial C_{se,p}}{\partial D_e}$; (d) Bode plot of normalized sensitivity transfer function of $\frac{\partial C_{se,p}}{\partial D_s}$

considered as adequate since the sensitivity starts to decay rapidly beyond 0.1 Hz. According to the plot, $\frac{\partial C_{se,p}}{\partial D_s}$ is sensitive to low frequency current input, as the magnitude is constant in low frequency range and drops quickly after the break frequency at between 0.01 and 0.1 Hz. This observation is consistent with the well-known battery Electrochemical Impedance Spectroscopy (EIS) results [34], which attribute the low frequency tail of the Nyquist plot to solid-phase diffusion. Furthermore, the theoretic value of the break frequency between the low-frequency sensitive range and high-frequency insensitive range for D_s can be estimated from the Bode plot and Eqn. (30). The magnitude plot can be approximated by two line segments as shown in Fig. 3a. The low-frequency segment 'L1' is found by taking the magnitude of the frequency response to $\omega = 0$,

$$|G_1(j\omega)| = \lim_{\omega \rightarrow 0} \left| \frac{\frac{\partial C_{se,p}}{\partial D_s} D_s}{I} (j\omega) \right| = \frac{R_s^2}{15F\varepsilon_s A \delta D_s} \quad (31)$$

The high-frequency segment 'L2' can be obtained by taking the frequency response to $\omega = \infty$,

$$|G_2(j\omega)| = \lim_{\omega \rightarrow \infty} \left| \frac{\frac{\partial C_{se,p}}{\partial D_s} D_s}{I} (j\omega) \right| = \frac{903D_s}{F\varepsilon_s A \delta R_s^2 \omega^2} \quad (32)$$

The break frequency ω_b is the intersection of the two segments, obtained by equating Eqn. (31) with (32),

$$\omega_b = \frac{116D_s}{R_s^2} \quad (33)$$

This result indicates that the sensitive frequency range of the diffusion coefficient depends on D_s and the particle radius R_s . Interestingly, it has been found in EIS study that there is a transition frequency in the

low-frequency tail portion of the Nyquist plot, which indicates the transition from semi-infinite diffusion to finite-space diffusion [35]. The transition frequency takes a similar form as Eqn. (33) [35,36], indicating possible correlation between the two which remains to be identified. These analytical results provide useful insights for experiment/input design to optimize the estimation accuracy of D_s .

The sensitivity transfer function can be easily converted to state space representation in time domain, e.g. through the canonical form as

$$\begin{bmatrix} \dot{x}_1 \\ \dot{x}_2 \\ \dot{x}_3 \\ \dot{x}_4 \end{bmatrix} = \begin{bmatrix} 0 & 1 & 0 & 0 \\ 0 & 0 & 1 & 0 \\ 0 & 0 & 0 & 1 \\ -\frac{12006225D_s^4}{R_s^8} & -\frac{1309770D_s^3}{R_s^6} & -\frac{42651D_s^2}{R_s^4} & -\frac{378D_s}{R_s^2} \end{bmatrix} \begin{bmatrix} x_1 \\ x_2 \\ x_3 \\ x_4 \end{bmatrix} + \begin{bmatrix} 0 \\ 0 \\ 0 \\ 1 \end{bmatrix} I \quad (34)$$

$$\frac{\partial C_{se}(t)}{\partial D_s} = \frac{21}{F\varepsilon_s A \delta R_s^6} [38115D_s^2 \ 1980D_s R_s^2 \ 43R_s^4 \ 0] \begin{bmatrix} x_1 \\ x_2 \\ x_3 \\ x_4 \end{bmatrix} \quad (35)$$

The formula can be used to compute the sensitivity of D_s under any current input $I(t)$ in real time efficiently. We will compare the results of the analytic derivation based on SPMe with numerical simulation of the sensitivity differential equations (SDE) based on the original full-order P2D model in Section 5 for verification.

4.2. Sensitivity of active material volume fraction ε_s

According to Eqn. (25), the active material volume fraction ε_s affects V through the lumped Ohmic resistance, open circuit potential U , and the overpotential η . Hence the sensitivity is obtained by applying the chain rule of differentiation as

$$\frac{\partial V}{\partial \varepsilon_s} = \frac{\partial R_\Omega}{\partial \varepsilon_s} I + \frac{\partial \eta}{\partial a_s} \frac{\partial a_s}{\partial \varepsilon_s} + \left(\frac{\partial \eta}{\partial c_{se}} + \frac{\partial U}{\partial c_{se}} \right) \frac{\partial c_{se}}{\partial \varepsilon_s}, \quad (36)$$

which consists of four terms. The first term, $\frac{\partial R_\Omega}{\partial \varepsilon_s} I$, is the linear non-dynamic term which reflects the impact of ε_s on the resistance of SEI. It can be obtained by differentiating Eqn. (26) to ε_s as

$$\frac{\partial R_\Omega}{\partial \varepsilon_s} = \frac{-R_f R_s}{3A \delta \varepsilon_s^2} \quad (37)$$

The second term, $\frac{\partial \eta}{\partial a_s} \frac{\partial a_s}{\partial \varepsilon_s}$, is the nonlinear non-dynamic terms that can be derived by differentiating Eqn. (20) to ε_s and substituting j^{Li} with I based on Eqn. (4),

$$\frac{\partial \eta}{\partial a_s} \frac{\partial a_s}{\partial \varepsilon_s} = \frac{-RT}{\alpha_a F \varepsilon_s} \frac{\text{sign}(I)}{\sqrt{1 + \frac{1}{\varepsilon_s^2}}} = \frac{-RT}{\alpha_a F \varepsilon_s} \frac{\text{sign}(I)}{\sqrt{1 + \left(\frac{6\varepsilon_s i_0 A \delta}{IR_s} \right)^2}} \quad (38)$$

It is seen that $\frac{\partial \eta}{\partial a_s} \frac{\partial a_s}{\partial \varepsilon_s}$ is a nonlinear function of current I , and changes instantaneously with current. The remaining two terms are the semi-linear dynamic terms of the ε_s sensitivity. Specifically, the third term $\frac{\partial \eta}{\partial c_{se}} \frac{\partial c_{se}}{\partial \varepsilon_s}$ represents the impact of ε_s on the exchange current i_0 which affects the overpotential through the particle surface concentration c_{se} , where the nonlinear coefficient $\frac{\partial \eta}{\partial c_{se}}$ has been obtained in Eqn. (29). The fourth term, $\frac{\partial U}{\partial c_{se}} \frac{\partial c_{se}}{\partial \varepsilon_s}$ accounts for the impact of ε_s on open circuit potential (OCP) through the particle surface concentration c_{se} .

The state sensitivity $\frac{\partial c_{se}}{\partial \varepsilon_s}$ can be derived using the same method for deriving $\frac{\partial c_{se}}{\partial D_e}$. Specifically, by taking the partial derivative of c_{se} to ε_s in Eqn. (7), the sensitivity transfer function of $\frac{\partial c_{se}}{\partial \varepsilon_s}$ can be obtained as

$$\frac{\partial C_{se}}{\partial \varepsilon_s}(s) = \left[\frac{7R_s^4 s^2 + 420D_s R_s^2 s + 3465D_s^2}{Fs(R_s^4 s^2 + 189D_s R_s^2 s + 3465D_s^2)} \right] \frac{I(s)}{\varepsilon_s^2 A \delta} \quad (39)$$

For frequency domain analysis, the Bode plot of the normalized sensitivity, $\frac{\partial C_{se,p}}{\partial \varepsilon_s}(s) \cdot \varepsilon_{s,p}$, is shown in Fig. 3b. It is seen that the analytic STF derived based on the 3rd order Padé approximation matches well with the sensitivity of the original transcendental transfer function, especially in the frequency range below 0.1 Hz. The mismatch beyond that frequency is less of a concern due to the significant attenuation. It is interesting to note that the frequency response of $\frac{\partial c_{se}}{\partial \varepsilon_s}$ is fundamentally different from that of $\frac{\partial c_{se}}{\partial D_e}$ shown in Fig. 3a. Instead of remaining constant in low frequency range and rolling off after the break frequency, $\frac{\partial c_{se}}{\partial \varepsilon_s}$ shows a monotonically decreasing trend over the whole frequency range due to the fact that $\frac{\partial c_{se}}{\partial \varepsilon_s}(s)$ contains a pole at $s = 0$ according to Eqn. (39). This observation reveals the distinctive dynamic nature of the sensitivity of different parameters and demonstrates the necessity of studying them respectively. The implication of different sensitivity dynamics will be analyzed in the subsequent section in detail.

4.3. Sensitivity of reaction rate constant k

Reaction rate constant k affects the terminal voltage V solely through the over-potential η , and hence the sensitivity is obtained by differentiating Eqn. (25) to k ,

$$\frac{\partial V(t)}{\partial k} = \frac{\partial \eta(t)}{\partial k}, \quad (40)$$

which is a nonlinear non-dynamic term

$$\frac{\partial \eta}{\partial k} = \frac{\partial \eta}{\partial \xi} \left(\frac{\partial \xi}{\partial k} \right) = \frac{-RT}{\alpha_a F k} \frac{\text{sign}(I)}{\sqrt{1 + \frac{1}{\varepsilon_s^2}}} = \frac{-RT}{\alpha_a F k} \frac{\text{sign}(I)}{\sqrt{1 + \left(\frac{6\varepsilon_s i_0 A \delta}{IR_s} \right)^2}} \quad (41)$$

It is noted that the normalized sensitivity $\frac{\partial \eta(t)}{\partial k}$ is essentially the same

as the normalized $\frac{\partial \eta(t)}{\partial a_s} \frac{\partial a_s}{\partial \varepsilon_s}$, and hence their behavior is similar.

4.4. Sensitivity of electrolyte diffusion coefficient D_e

According to Eqn. (8), the electrolyte diffusion coefficient D_e governs the evolution of the electrolyte concentration c_e . The c_e gradient induces potential difference across the electrodes, which affects the battery terminal voltage. Therefore, by applying the chain rule of differentiation to Eqn. (25), the sensitivity of D_e takes the form of a semi-linear dynamic term,

$$\begin{aligned} \frac{\partial V}{\partial D_e} &= \frac{\partial \Delta \varphi_{e,con}}{\partial D_e} = \frac{\partial \Delta \varphi_{e,con}}{\partial c_e} \frac{\partial c_e}{\partial D_e} \\ &= \frac{2RT(1 - t_+^0)}{F} (1 + \gamma) \left(\frac{1}{c_{e,p}} \frac{\partial c_{e,p}}{\partial D_e} - \frac{1}{c_{e,n}} \frac{\partial c_{e,n}}{\partial D_e} \right) \end{aligned} \quad (42)$$

For state sensitivity $\frac{\partial c_e}{\partial D_e}$, similar to $\frac{\partial c_{se}}{\partial \varepsilon_s}$, we can derive a sensitivity transfer function by taking the partial derivative of Eqn. (11) to D_e ,

$$\begin{aligned} \frac{\partial C_{e,i}}{\partial D_e}(s) &= \frac{\frac{(e_e^{1.5} + 4e_e^{1.5})}{8 \times 10^9 FAD_e^2 e_e^{1.5} e_{sep}^{1.5}} I(s)}{\frac{(e_e^2 e_{sep}^{1.5} + 24e_e^3 + 320e_e^3 e_{sep}^{1.5} + 160e_e^{1.5} e_e^{1.5} e_{sep}^{1.5})^2}{3.6864 \times 10^{20} (4D_e e_e^{0.5} e_{sep}^3 + D_e e_e^2 e_{sep}^{1.5})^2} s^2 + \frac{(e_e^2 e_{sep}^{1.5} + 24e_e^3 + 320e_e^3 e_{sep}^{1.5} + 160e_e^{1.5} e_e^{1.5} e_{sep}^{1.5})}{9.6 \times 10^9 (4D_e e_e^{0.5} e_{sep}^3 + D_e e_e^2 e_{sep}^{1.5})} s + 1} \end{aligned} \quad (43)$$

In frequency domain, the dynamic nature of (normalized) $\frac{\partial c_e}{\partial D_e}$ can be studied based on the Bode plot shown in Fig. 3c. The blue line stands for the frequency response of the analytic STF, and the red line represents the sensitivity calculated based on the original transcendental transfer function. The two match well at low frequency up to around 0.1 Hz, after which both start to decay rapidly. It can be seen that $\frac{\partial c_e}{\partial D_e}$ is sensitive to low frequency current input, and the theoretic value of the break frequency between the low-frequency sensitive range and high-frequency insensitive range can be estimated from the STF. The sensitivity transfer function can be easily converted to state space representation in time domain to calculate the sensitivity $\frac{\partial c_e}{\partial D_e}$ under generic current input I .

4.5. Sensitivity of porosity ε_e

According to Eqns. (14)–(16), the porosity ε_e affects the terminal voltage V through the electrolyte concentration polarization potential $\Delta \varphi_{e,con}$ in Eqn (15) and the ohmic polarization potential IR_Ω in Eqn. (25). Hence the sensitivity is obtained by applying the chain rule of differentiation to Eqn. (25) as

$$\frac{\partial V}{\partial \varepsilon_e} = \frac{\partial R_\Omega}{\partial \varepsilon_e} I + \frac{\partial \Delta \varphi_{e,con}}{\partial \varepsilon_e} \frac{\partial c_e}{\partial \varepsilon_e}, \quad (44)$$

which consists of two terms. The first term, $\frac{\partial R_\Omega}{\partial \varepsilon_e} I$, is the linear non-dynamic term related to the ohmic resistance of the electrolyte, which can be derived by differentiating Eqn. (26) to ε_e as

$$\frac{\partial R_\Omega}{\partial \varepsilon_e} = \frac{0.75(\delta_p + \delta_n)}{\kappa \varepsilon_e^{2.5} A} \quad (45)$$

The second term, $\frac{\partial \Delta \varphi_{e,con}}{\partial \varepsilon_e} \frac{\partial c_e}{\partial \varepsilon_e}$, is the semi-linear dynamic term, which captures the impact of ε_e on $\Delta \varphi_{e,con}$ through the electrolyte concentration c_e . It can be derived by applying the chain rule of differentiation to Eqn. (25) as

$$\frac{\partial \Delta \varphi_{e,con}}{\partial \varepsilon_e} \frac{\partial c_e}{\partial \varepsilon_e} = \frac{2RT(1 - t_+^0)}{F} (1 + \gamma) \left(\frac{1}{c_{e,p}} \frac{\partial c_{e,p}}{\partial \varepsilon_e} - \frac{1}{c_{e,n}} \frac{\partial c_{e,n}}{\partial \varepsilon_e} \right) \quad (46)$$

Then, similar to $\frac{\partial c_e}{\partial D_e}$, the sensitivity transfer function of $\frac{\partial c_e}{\partial \varepsilon_e}$ can be obtained by taking the partial derivative of $C_e(s)$ to ε_e in Eqn. (11),

$$\frac{\partial C_{e,i}}{\partial \epsilon_e}(s) = \frac{\pm \left(\frac{6\epsilon_e^{4.5} + 320\epsilon_e^{4.5}\epsilon_{e,sep} + 76\epsilon_e^3\epsilon_{e,sep}^{1.5} + 240\epsilon_e^{1.5}\epsilon_{e,sep}^3 + 3\epsilon_e^2\epsilon_{e,sep}^{2.5}}{3.84 \times 10^{14} D_e^2 \epsilon_e^3 \epsilon_{e,sep}^3 (\epsilon_e^{1.5} + 4\epsilon_{e,sep}^{1.5})} s + \frac{3}{4 \times 10^4 (D_e \epsilon_e^{2.5})} \right)^{\frac{1-t_0^+}{FA}} I(s)}{\frac{(\epsilon_e^2 \epsilon_{e,sep} + 24\epsilon_e^3 + 320\epsilon_e^2 \epsilon_{e,sep} + 160\epsilon_e^{1.5} \epsilon_{e,sep}^2)^2}{3.6864 \times 10^{20} (4D_e \epsilon_e^{0.5} \epsilon_{e,sep}^3 + D_e \epsilon_e^2 \epsilon_{e,sep}^{1.5})^2} s^2 + \frac{(\epsilon_e^2 \epsilon_{e,sep} + 24\epsilon_e^3 + 320\epsilon_e^2 \epsilon_{e,sep} + 160\epsilon_e^{1.5} \epsilon_{e,sep}^2)^2}{9.6 \times 10^9 (4D_e \epsilon_e^{0.5} \epsilon_{e,sep}^3 + D_e \epsilon_e^2 \epsilon_{e,sep}^{1.5})} s + 1} \quad (47)$$

For frequency domain analysis, the Bode plot of (the normalized) STF of $\frac{\partial C_{e,i}}{\partial \epsilon_e}$ is shown in Fig. 3d. The analytic results based on the 1st order Padé approximation are in good agreement with the results based on the original transcendental transfer function. It is noted that the frequency response of $\frac{\partial C_{e,i}}{\partial \epsilon_e}$ is different from its solid-phase counterpart $\frac{\partial C_{se}}{\partial \epsilon_s}$, i.e. the active material volume fraction. Compared with $\frac{\partial C_{se}}{\partial \epsilon_s}(s)$ which decreases monotonically over frequency, $\frac{\partial C_{e,i}}{\partial \epsilon_e}(s)$ remains constant in the low frequency range. This is because $\frac{\partial C_{e,i}}{\partial \epsilon_e}(s)$ does not contain a pole at $s = 0$ as

$\frac{\partial C_{se}}{\partial \epsilon_s}(s)$ does. The root cause arises from the fundamental difference between the lithium diffusion in the solid phase through a spherical particle and that in the electrolyte phase along a straight line. Specifically, the spherical diffusion is cumulative as lithium ion will accumulate in the particle over time (indicated by the pole at $s = 0$ as an integrator), while the electrolyte diffusion is conservative as the total amount of lithium in the electrolyte remains constant. The sensitivity derivation of separator porosity $\epsilon_{e,sep}$ is similar to that of ϵ_e .

5. Verification of analytic derivation

In this section, we will verify the derived analytic expressions for the sensitivity of the solid-phase diffusion coefficient D_s , active material volume fraction ϵ_s , reaction rate constant k , electrolyte diffusion coefficient D_e , porosity ϵ_e and $\epsilon_{e,sep}$ against the exact sensitivity obtained from numerical simulation of a full order P2D model. The verification is performed under three different types of current profiles, namely the

constant-current (CC) discharging profiles, pulse profile, and a drive cycle, i.e. the Federal Urban Driving Schedule (FUDS). Under CC discharging, the battery initial SOC is set to 100%, and a constant current is applied to deplete the battery towards a final SOC of 0%. Simulation is repeated under 1–3 C constant current with the purpose of verifying the sensitivity over the whole SOC range under different current rates. Under FUDS simulation, battery is initialized to 70% SOC and then subject to the dynamic current profile shown in Fig. 4a. During the pulse current simulation as shown in Fig. 4b, battery is initialized to 50% SOC and then cycled under alternating 1C charging and discharging pulses, each of which lasts for 30 s and repeats over time. The FUDS and pulse tests are intended to verify the dynamics of sensitivity under varying input. The model parameters used in simulation are adopted from Ref. [33], and Fig. 4c shows the open circuit potential (OCP) slope of the cathode, of which the parameter sensitivity will be verified.

5.1. Numerical simulation of exact sensitivity based on full order P2D model

The sensitivity calculated based on the derived analytical expressions will be compared with the exact numerical computation based on the full order P2D model from which the SPM was derived previously in this paper. The P2D model-based sensitivity computation is performed by solving the Sensitivity Differential Algebraic Equations (SDAEs) derived from the full order model as in Ref. [30]. Specifically, the PDEs are first discretized spatially using the finite difference method or Padé approximation to formulate a system of continuous Differential Algebraic Equations (DAEs),

$$\dot{\mathbf{X}} = \mathbf{f}(\mathbf{X}, \mathbf{Z}, u, \lambda) \mathbf{0} = \mathbf{g}(\mathbf{X}, \mathbf{Z}, u, \lambda) \mathbf{y} = h(\mathbf{X}, \mathbf{Z}, u, \lambda) \quad (48)$$

where $\mathbf{X} = [\mathbf{c}_s, \mathbf{c}_e]^T \in \mathbb{R}^{n_x}$ denotes the state variables with \mathbf{c}_s and \mathbf{c}_e being the discretized state vectors, $\mathbf{Z} = [\varphi_s, i_e, \varphi_e, j^{Li}]^T \in \mathbb{R}^{n_z}$ represents the

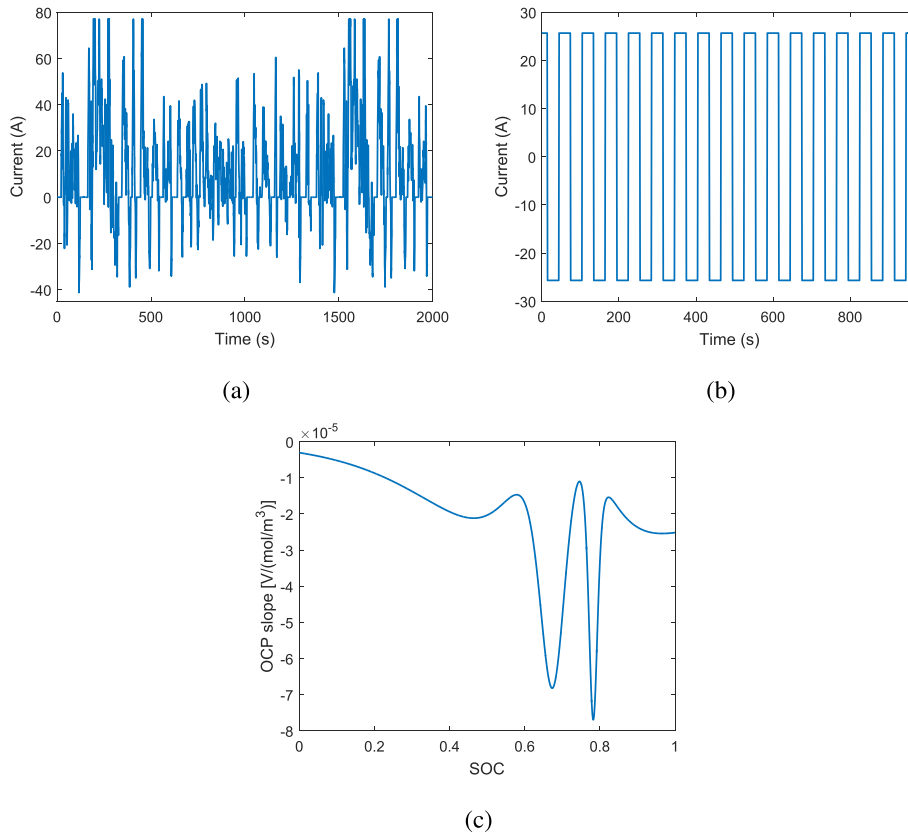


Fig. 4. (a) FUDS current profile; (b) Pulse current profile; (c) OCP slope of cathode.

algebraic states, $u = I(t)$ is the model input, and $y = V(t)$ is the voltage output. In addition, $\lambda = [D_s, D_e, \varepsilon_s, \varepsilon_e, k] \in \mathbb{R}^{np}$ denotes the target parameters for sensitivity analysis.

The SDAEs can then be formulated by taking the partial derivative of

Eqn. (48) to the target parameters λ [37],

$$\dot{\lambda}_\lambda = \mathbf{f}_X \mathbf{X}_\lambda + \mathbf{f}_Z \mathbf{Z}_\lambda + \mathbf{f}_\lambda 0 = \mathbf{g}_X \mathbf{X}_\lambda + \mathbf{g}_Z \mathbf{Z}_\lambda + \mathbf{g}_\lambda y_\lambda = h_X \mathbf{X}_\lambda + h_Z \mathbf{Z}_\lambda + h_\lambda \quad (49)$$

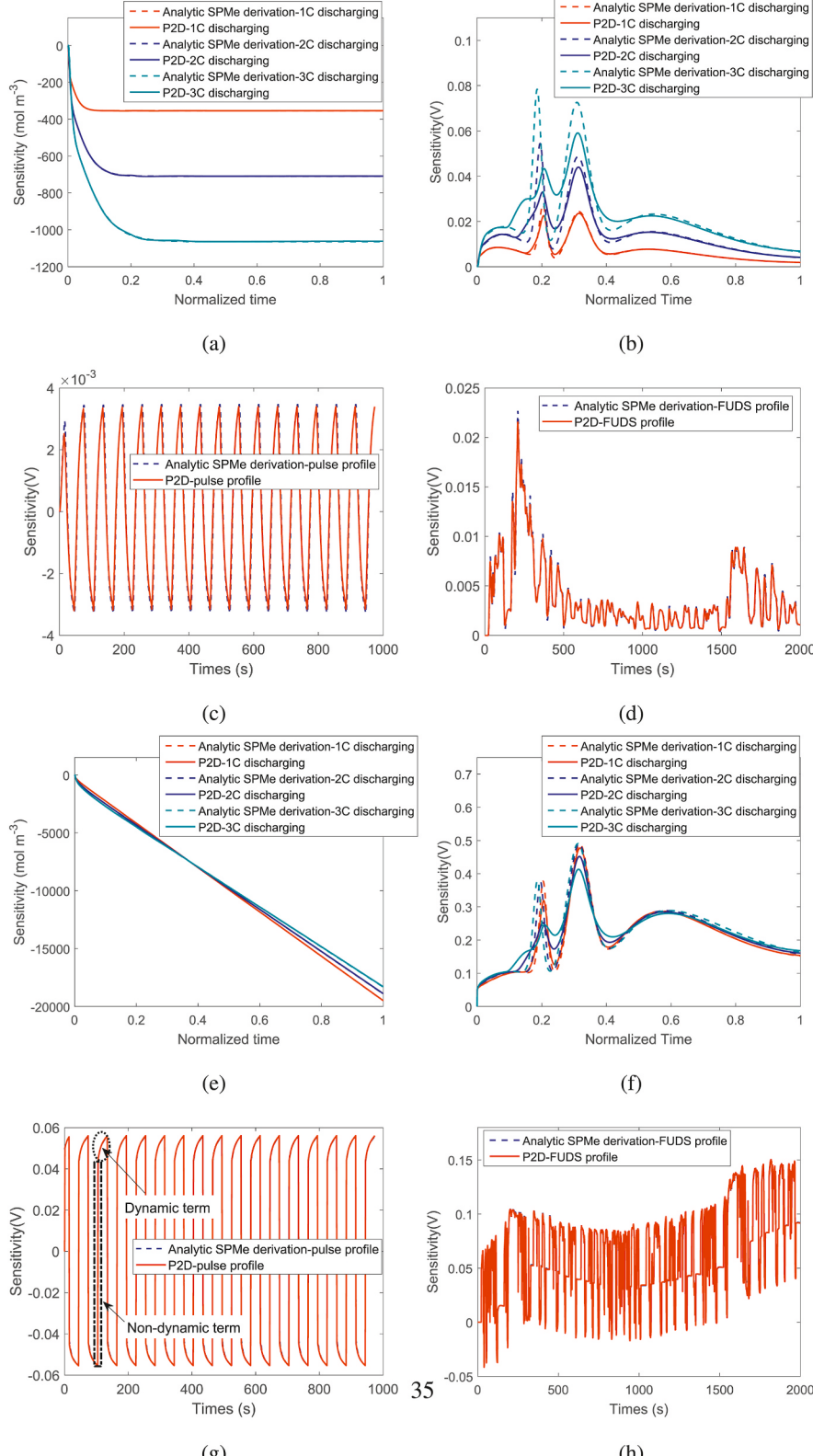


Fig. 5. (a) Normalized $\frac{\partial c_{se,p}}{\partial D_{sp}}$ under CC discharging; (b) Normalized $\frac{\partial V}{\partial D_{sp}}$ under CC discharging; (c) Normalized $\frac{\partial V}{\partial D_{sp}}$ under pulse profile; (d) Normalized $\frac{\partial V}{\partial D_{sp}}$ under FUDS; (e) Normalized $\frac{\partial c_{se,p}}{\partial \varepsilon_{sp}}$ under CC discharging; (f) Normalized $\frac{\partial V}{\partial \varepsilon_{sp}}$ under CC discharging; (g) Normalized $\frac{\partial V}{\partial \varepsilon_{sp}}$ under pulse profile; (h) Normalized $\frac{\partial V}{\partial \varepsilon_{sp}}$ under FUDS.

where $\mathbf{X}_\lambda = \frac{\partial \mathbf{X}}{\partial \lambda} \in \mathbb{R}^{n_X \times n_\lambda}$, $\mathbf{Z}_\lambda = \frac{\partial \mathbf{Z}}{\partial \lambda} \in \mathbb{R}^{n_Z \times n_\lambda}$, $\mathbf{y}_\lambda = \frac{\partial \mathbf{y}}{\partial \lambda} \in \mathbb{R}^{n_p}$, and $\mathbf{f}_X = \frac{\partial \mathbf{f}}{\partial X} \in \mathbb{R}^{n_X \times n_X}$, $\mathbf{f}_Z = \frac{\partial \mathbf{f}}{\partial Z} \in \mathbb{R}^{n_Z \times n_Z}$, and $\mathbf{f}_\lambda = \frac{\partial \mathbf{f}}{\partial \lambda} \in \mathbb{R}^{n_X \times n_\lambda}$ are the Jacobian matrices of f with respect to \mathbf{X} , \mathbf{Z} , and λ respectively. Similarly, the Jacobian matrices of the functions \mathbf{g} and h with respect to \mathbf{X} , \mathbf{Z} , and λ are represented by \mathbf{g}_X , \mathbf{g}_Z , \mathbf{g}_λ , \mathbf{h}_X , \mathbf{h}_Z , and \mathbf{h}_λ respectively.

Solving the DAE system in Eqns. (48) and (49) could render the exact parameter sensitivity y_λ , but is subject to significant computation complexity as the total number of equations is typically in the order of hundreds depending on the number of discretization. A simulation platform has been developed to solve the DAE system by integrating the open source software CasADi [38], which calculates the Jacobians using automatic differentiation, and the SUNDIAL IDA solver [39], which solves the resultant DAEs and SDAEs. More details can be found in Ref. [40].

5.2. Verification of sensitivity for solid-phase diffusion coefficient D_s

The verification results for the cathode diffusion coefficient $D_{s,p}$ are presented in Fig. 5a -5d. All sensitivity results have been normalized by multiplying with the nominal value of the parameter. It is seen that in all cases, the analytic derivation matches well with the P2D simulation. Fig. 5a-d demonstrate the verification results under CC discharging, among which Fig. 5a shows the state sensitivity $\frac{\partial c_{se,p}}{\partial D_{s,p}}$ and Fig. 5d presents the voltage sensitivity $\frac{\partial V}{\partial D_{s,p}}$. The time duration is normalized to $[0, 1]$ so that the 3 discharging cases can be presented over the same scale. Under CC discharging, the magnitude of $\frac{\partial c_{se,p}}{\partial D_{s,p}}$ sees significant increase for the first 250 s before reaching steady state. As shown in Fig. 5a, the analytic STF derived in Eqn. (30) characterizes both the transient and steady state, and matches the P2D simulation results very well (which is the average $\frac{\partial c_{se,p}}{\partial D_{s,p}}$ over the electrode). The resultant voltage sensitivity, $\frac{\partial V}{\partial D_{s,p}}$, is plotted in Fig. 5b, and shows good match between the analytic derivation and P2D simulation. The evolution of $\frac{\partial V}{\partial D_{s,p}}$ over time exhibits a “double-peak” trend, which is similar to the profile of the open circuit potential slope $\frac{\partial U_p}{\partial c_{se,p}}$ shown in Fig. 4c, because $\frac{\partial V}{\partial D_{s,p}}$ is dominated by the product of $\frac{\partial c_{se,p}}{\partial D_{s,p}}$ and $\frac{\partial U_p}{\partial c_{se,p}}$. Some discrepancies can be observed, which are attributed to the development of c_s gradient across the electrode neglected by the single particle assumption. The discrepancies are minimal under 1C current and increase under higher current due to more prominent concentration gradient. It is noted that such discrepancies are not seen in $\frac{\partial c_{se,p}}{\partial D_{s,p}}$ because Fig. 5a shows the average $\frac{\partial c_{se,p}}{\partial D_{s,p}}$ over the electrode for the P2D results. Fig. 5c demonstrates the verification results under the pulse current, in which the sensitivity fluctuates as the current changes direction periodically. The analytic derivation matches almost perfectly with P2D simulation because the lithium concentration gradient would not build up during fast transient. Fig. 5d demonstrates the results under the FUDS drive cycle. It is seen that the voltage sensitivity of D_s varies significantly under real-world operation as some data segments are highly sensitive/insensitive to D_s compared to others. By correlating to the results under CC discharging, it is figured that high D_s sensitivity can be achieved under current patterns with high magnitude and adequate duration, which explains the two sensitivity peaks at around 250s and 1600s in Fig. 5d.

5.3. Sensitivity verification for active material volume fraction ε_s

The sensitivity verification results for the cathode active material volume fraction $\varepsilon_{s,p}$ are presented in Fig. 5e-5h under the CC discharging, pulse current, and FUDS profiles respectively. It can be seen that in all these cases, the analytic results derived based on SPM e match well with those from numerical P2D simulation. Furthermore, several interesting observations can be made. Under CC discharging, as seen in

Fig. 5e, the magnitude of the state sensitivity $\frac{\partial c_{se,p}}{\partial \varepsilon_{s,p}}$ keeps increasing over time, as opposed to the previous $\frac{\partial c_{se}}{\partial D_s}$, which reaches a finite steady state. This is theoretically predicted by the derived sensitivity transfer function in Eqn. (39), which contains a pole at 0, representing the integration of current over time. The voltage sensitivity $\frac{\partial V}{\partial \varepsilon_s}$, as shown in Fig. 5f, is dominated by the ever-increasing semi-linear dynamic term $\frac{\partial U_p}{\partial c_{se,p}} \cdot \frac{\partial c_{se,p}}{\partial \varepsilon_{s,p}}$, and hence shows the profile of the OCP slope. It is also interesting to note that the dependence of ε_s sensitivity on current magnitude is much weaker than that of D_s . The separation of the different terms of $\frac{\partial V}{\partial \varepsilon_s}$ can be observed more clearly from the pulse current simulation. As shown in Fig. 5g, the instantaneous jumps occurring at the periodic current switching indicates the non-dynamic terms $\frac{\partial \eta}{\partial a_{s,p}} \frac{\partial a_{s,p}}{\partial \varepsilon_{s,p}}$ and $\frac{\partial R_\Omega}{\partial \varepsilon_{s,p}}$, and the subsequent transient is dominated by the dynamic terms $\left(\frac{\partial U}{\partial c_{se}} + \frac{\partial \eta}{\partial c_{se}} \right) \frac{\partial c_{se}}{\partial \varepsilon_s}$.

It is seen that the derived analytic expressions not only enable fast and efficient computation of sensitivity, but also provide theoretic insight and explanation, which are unavailable from numerical simulation.

5.4. Verification of sensitivity for reaction rate constant k

The verification results for the reaction rate constant k are presented in Fig. 6a-6c. It can be seen that the analytic sensitivity derived based on SPM e matches well with the P2D numerical simulation under all current profiles. The parameter k affects the battery voltage through the overpotential η , and its sensitivity $\frac{\partial V}{\partial k}$ has been shown in Eqn. (41) as a nonlinear function of the input current I . Therefore, it is seen that the sensitivity of k evolves over time in similar patterns as the current variation under all profiles. In addition, the dependence of $\frac{\partial V}{\partial k}$ on lithium concentration (through the exchange current i_0) is minimal (at least under the given battery parameters considered in this paper), which makes $\frac{\partial V}{\partial k}$ remain constant over time under constant current.

5.5. Verification of sensitivity for electrolyte diffusion coefficient D_e

The verification results for the electrolyte diffusion coefficient D_e are presented in Fig. 7a -7d. Fig. 7a shows the evolution of the state sensitivity $\frac{\partial c_{e,p}}{\partial D_e}$ under CC discharging. According to the derived STF in Eqn. (43), the dynamics of $\frac{\partial c_{e,p}}{\partial D_e}$ feature a stable second order transfer function. Accordingly, it is shown in Fig. 7a that the sensitivity reaches a constant value after the initial transient. The analytic derivation based on SPM e matches fairly well with the numerical sensitivity from P2D simulation. Fig. 7b compares the voltage sensitivity $\frac{\partial V}{\partial D_e}$ under CC discharging profiles. It is seen that the mismatch between the analytic results based on SPM e and those from P2D simulation becomes more prominent. Nevertheless, the analytic results derived based on SPM e could match the exact sensitivity (from P2D simulation) well under low current and capture the main trend and feature under high current. Fig. 7c and 7d demonstrate the comparison of normalized $\frac{\partial V}{\partial D_e}$ under pulse and FUDS profiles, showing similar results. Under the FUDS profile, similar to the sensitivity results of D_s in Fig. 5d, the two peaks of high sensitivity are achieved under high magnitude current with adequate duration.

It is noted that the derived analytic sensitivity based on SPM e for D_e (and also the subsequent ε_e) in general does not match the P2D simulation as well as the electrode parameters D_s and ε_s . There are two possible model simplification steps involving the electrolyte submodel that may have led to the deviation/errors. The first one is the single particle assumption, which neglects the non-uniform distribution of the current density j^{Li} across the electrode in Eqn. (8), and the second one is the Pade approximation, which reduces the transcendental transfer function of the electrolyte concentration c_e to a 1st order rational transfer function. The main source of error can be identified as the first one, i.e. single particle assumption, since it is shown in Fig. 3c and d that

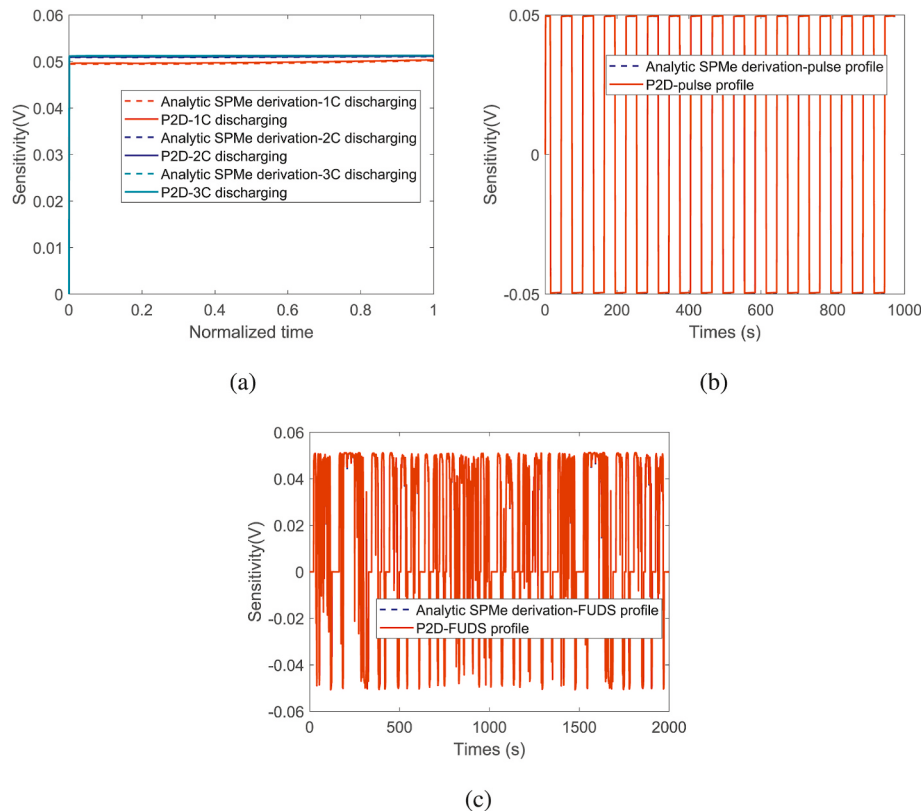


Fig. 6. (a) Normalized $\frac{\partial V}{\partial k_p}$ under CC discharging; (b) Normalized $\frac{\partial V}{\partial k_p}$ under pulse profile; (c) Normalized $\frac{\partial V}{\partial k_p}$ under FUDS.

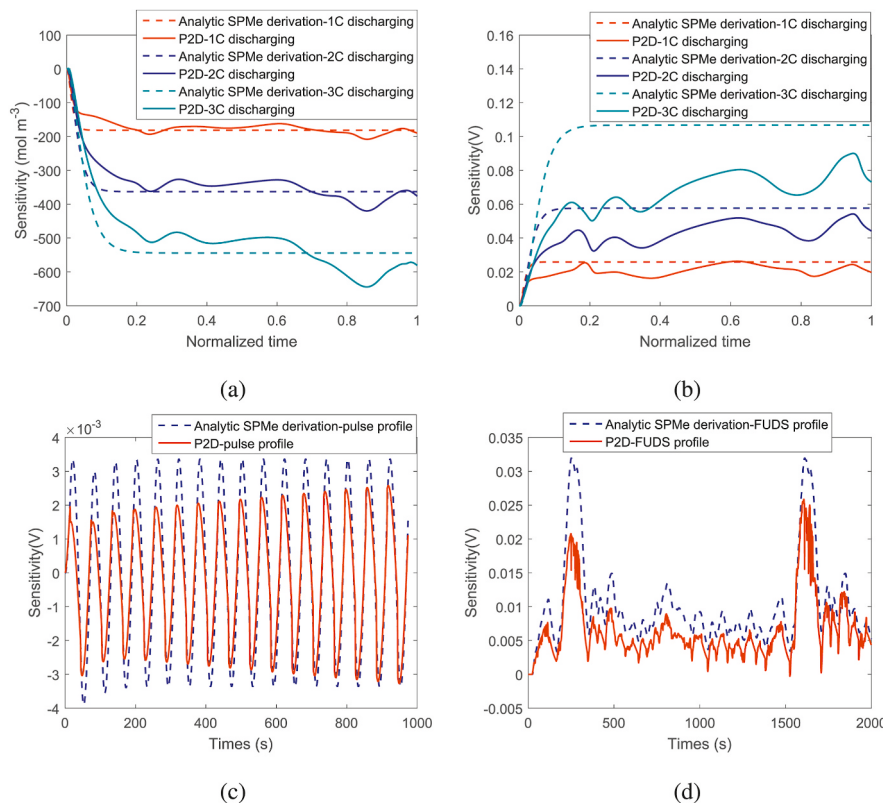


Fig. 7. (a) Normalized $\frac{\partial c_{sp}}{\partial D_e}$ under CC discharging; (b) Normalized $\frac{\partial V}{\partial D_e}$ under CC discharging; (c) Normalized $\frac{\partial V}{\partial D_e}$ under pulse profile; (d) Normalized $\frac{\partial V}{\partial D_e}$ under FUDS.

the 1st order Pade approximation matches well with the transcendental transfer function. The main reason for the larger deviation under the single particle assumption for the electrolyte submodel is that the uniform-current-density approximation affects both the source term and

the boundary conditions of the electrolyte diffusion in Eqn. (8). In order to mitigate the deviation, other methods of model reduction can be used to simplify the original full order model without relying on the single particle assumption, such as the balanced truncation, proper orthogonal

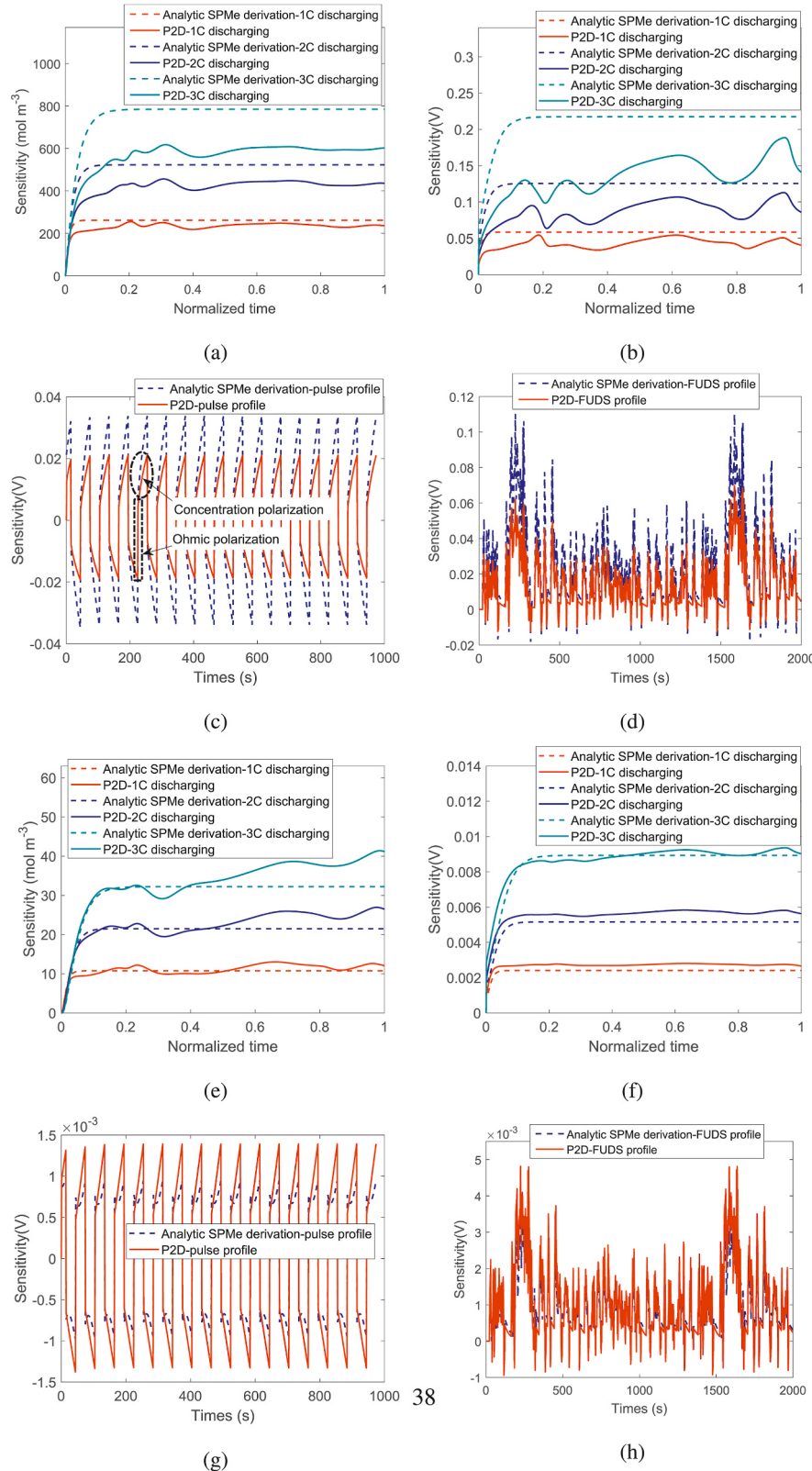


Fig. 8. (a) Normalized $\frac{dC_{e,p}}{dt_e}$ under CC discharging; (b) Normalized $\frac{dV}{dt_e}$ under CC discharging; (c) Normalized $\frac{dV}{dt_e}$ under pulse profile; (d) Normalized $\frac{dV}{dt_e}$ under FUDS; (e) Normalized $\frac{dC_{e,p}}{dt_{e,sep}}$ under CC discharging; (f) Normalized $\frac{dV}{dt_{e,sep}}$ under CC discharging; (g) Normalized $\frac{dV}{dt_e}$ under pulse profile; (h) Normalized $\frac{dV}{dt_{e,sep}}$ under FUDS.

decomposition (POD), and the Galerkin method among others [41]. However, these methods are highly complicated and/or non-analytical, and hence make it impossible/difficult to further derive the parameter sensitivity, suggesting an interesting topic for future research.

5.6. Verification of sensitivity for electrode porosity ε_e

The verification results for the electrode porosity ε_e are presented in Fig. 8a -8d. The state sensitivity $\frac{\partial c_{ep}}{\partial \varepsilon_e}$ at the cathode boundary ($x = L_c$) under CC discharging is shown in the Fig. 8a, which is approximated well by the second order STF derived based on SPM_e under low current, e.g. 1C. The mismatch becomes prominent under higher C rates due to the aforementioned assumption and approximation of the electrolyte model. Fig. 8b shows similar results for the voltage sensitivity $\frac{\partial V}{\partial \varepsilon_e}$. According to Eqn. (36), ε_e affects the terminal voltage through two terms, i.e. the linear non-dynamic electrolyte ohmic polarization $\varphi_{e,\Omega}$ and the semi-linear dynamic concentration polarization $\Delta\varphi_{e,con}$. The effects of these two terms are clearly distinguishable under the pulse current shown in Fig. 8c. The instantaneous jump, which occurs every time when current switches direction, corresponds to the Ohmic polarization term, and the subsequent transient indicates the concentration polarization. The results under dynamic current profiles shown in Fig. 8c and d are similar to those under CC discharging, as the analytic sensitivity derived based on SPM_e captures the main trend and features of the numerical sensitivity from P2D simulation while sees discrepancy especially under high current.

5.7. Verification of sensitivity for separator porosity $\varepsilon_{e,sep}$

The dynamics of the sensitivity of the separator porosity $\varepsilon_{e,sep}$ are similar to those of the electrode porosity ε_e as shown in Fig. 8e–8h. However, it is noted that the SPM_e results match the P2D simulation much better than in the case of ε_e , which can be explained by two reasons. First, the intercalation current density is zero in the separator due to the absence of intercalation reaction, and hence the electrolyte diffusion dynamics does not suffer from the uniform current density assumption. Second, the separator only accounts for a small portion of the total volume of the battery (e.g. 11% under the given parameters considered in this paper). Therefore, the lithium ion concentration gradient would not build up significantly across the separator. Meanwhile, since the volume of the separator is much smaller than that of the electrodes, the sensitivity of $\varepsilon_{e,sep}$ is also much smaller in magnitude than that of ε_e .

6. Conclusions

In this paper, we study the analytic derivation and analysis of the sensitivity of battery electrochemical parameters. It is shown that the parameter sensitivity typically consists of different terms featuring linear/nonlinear and dynamic/non-dynamic properties due to the effect of different voltage components. A framework is proposed to derive different sensitivity terms based on model reformulation, approximation, and simplification techniques. The derived analytic expressions have been verified through comparison with the exact numerical computation based on a full-order P2D model, showing satisfactory fidelity under typical operating scenarios.

The derived analytic results could significantly benefit the emerging research on data optimization for battery state and parameter estimation. As indicated by their distinctive sensitivity dynamics, different parameters are associated with different data patterns that would yield optimal sensitivity/estimation accuracy. For offline model identification, the analytic expression will enable direct optimization of the input excitation, which is currently intractable due to the computational complexity [30]. Preliminary results have been obtained and demonstrated in an upcoming publication [42]. For real-time state estimation

and parameter learning, fast and efficient computation of sensitivity using the analytic expressions will facilitate the selection/mining of sensitive data from random online data stream. Using these data for estimation could enhance the accuracy and robustness of the results [23].

Declaration of competing interest

The authors declare that they have no known competing financial interests or personal relationships that could have appeared to influence the work reported in this paper.

CRediT authorship contribution statement

Qingzhi Lai: Methodology, Software, Conceptualization, Validation, Data curation, Writing - original draft, Writing - review & editing. **Sidharth Jangra:** Software, Validation, Writing - original draft. **Hyoung Jun Ahn:** Validation. **Geumbee Kim:** Software, Validation. **Won Tae Joe:** Project administration, Funding acquisition, Conceptualization. **Xinfan Lin:** Conceptualization, Supervision, Project administration, Funding acquisition, Writing - original draft, Writing - review & editing, Resources.

Acknowledgment

The authors appreciate the funding support from LG Chem Ltd. through the LG Chem BIC program.

References

- [1] M. Doyle, T.F. Fuller, J. Newman, Modeling of galvanostatic charge and discharge of the lithium/polymer/insertion cell, *J. Electrochem. Soc.* 140 (6) (1993) 1526.
- [2] L. Lu, X. Han, J. Li, J. Hua, M. Ouyang, A review on the key issues for lithium-ion battery management in electric vehicles, *J. Power Sources* 226 (2013) 272–288.
- [3] X. Lin, Y. Kim, S. Mohan, J.B. Siegel, A.G. Stefanopoulou, Modeling and estimation for advanced battery management, *Annu. Rev. Contr. Robot. Autonom. Syst.* 2 (2019) 393–426.
- [4] N. Michel, A.K. Sinha, Z. Kong, X. Lin, Multiphysical modeling of energy dynamics for multirotor unmanned aerial vehicles, in: 2019 International Conference on Unmanned Aircraft Systems (ICUAS), IEEE, 2019, pp. 738–747.
- [5] X. Hu, S. Li, H. Peng, A comparative study of equivalent circuit models for li-ion batteries, *J. Power Sources* 198 (2012) 359–367.
- [6] X. Lin, H.E. Perez, S. Mohan, J.B. Siegel, A.G. Stefanopoulou, Y. Ding, M. P. Castanier, A lumped-parameter electro-thermal model for cylindrical batteries, *J. Power Sources* 257 (2014) 1–11.
- [7] T.F. Fuller, M. Doyle, J. Newman, Simulation and optimization of the dual lithium ion insertion cell, *J. Electrochem. Soc.* 141 (1) (1994) 1–10.
- [8] D. Di Domenico, A. Stefanopoulou, G. Fiengo, Lithium-ion battery state of charge and critical surface charge estimation using an electrochemical model-based extended kalman filter, *J. Dyn. Syst. Meas. Contr.* 132 (6) (2010).
- [9] J. Marcicki, M. Canova, A.T. Conlisk, G. Rizzoni, Design and parametrization analysis of a reduced-order electrochemical model of graphite/lifepo4 cells for soc/soh estimation, *J. Power Sources* 237 (2013) 310–324.
- [10] G.L. Plett, Extended kalman filtering for battery management systems of libp-based hev battery packs Part 3. state and parameter estimation, *J. Power Sources* 134 (2) (2004) 277–292.
- [11] A.M. Bizeray, S. Zhao, S.R. Duncan, D.A. Howey, Lithium-ion battery thermal-electrochemical model-based state estimation using orthogonal collocation and a modified extended kalman filter, *J. Power Sources* 296 (2015) 400–412.
- [12] X. Lin, A.G. Stefanopoulou, Y. Li, R.D. Anderson, State of charge imbalance estimation for battery strings under reduced voltage sensing, *IEEE Trans. Contr. Syst. Technol.* 23 (3) (2014) 1052–1062.
- [13] X. Hu, D. Cao, B. Egardt, Condition monitoring in advanced battery management systems: Moving horizon estimation using a reduced electrochemical model, *IEEE ASME Trans. Mechatron.* 23 (1) (2017) 167–178.
- [14] S.J. Moura, N.A. Chaturvedi, M. Krstic, Adaptive partial differential equation observer for battery state-of-charge/state-of-health estimation via an electrochemical model, *J. Dyn. Syst. Meas. Contr.* 136 (1) (2014).
- [15] S.-X. Tang, L. Camacho-Solorio, Y. Wang, M. Krstic, State-of-charge estimation from a thermal-electrochemical model of lithium-ion batteries, *Automatica* 83 (2017) 206–219.
- [16] S. Dey, B. Ayalew, P. Pisu, Nonlinear robust observers for state-of-charge estimation of lithium-ion cells based on a reduced electrochemical model, *IEEE Trans. Contr. Syst. Technol.* 23 (5) (2015) 1935–1942.
- [17] X. Lin, A.G. Stefanopoulou, Analytic bound on accuracy of battery state and parameter estimation, *J. Electrochem. Soc.* 162 (9) (2015) A1879–A1891.

- [18] P.P. Mishra, M. Garg, S. Mendoza, J. Liu, C.D. Rahn, H.K. Fathy, How does model reduction affect lithium-ion battery state of charge estimation errors? theory and experiments, *J. Electrochem. Soc.* 164 (2) (2017) A237–A251.
- [19] X. Lin, Theoretical analysis of battery soc estimation errors under sensor bias and variance, *IEEE Trans. Ind. Electron.* 65 (9) (2018) 7138–7148.
- [20] H.E. Perez, J.B. Siegel, X. Lin, A.G. Stefanopoulou, Y. Ding, M.P. Castanier, Parameterization and validation of an integrated electro-thermal cylindrical lfp battery model, in: ASME 2012 5th Annual Dynamic Systems and Control Conference Joint with the JSME 2012 11th Motion and Vibration Conference, American Society of Mechanical Engineers Digital Collection, 2012, pp. 41–50.
- [21] Z. He, G. Yang, L. Lu, A parameter identification method for dynamics of lithium iron phosphate batteries based on step-change current curves and constant current curves, *Energies* 9 (6) (2016) 444.
- [22] J.C. Forman, S.J. Moura, J.L. Stein, H.K. Fathy, Genetic identification and Fisher identifiability analysis of the doyle–fuller–newman model from experimental cycling of a lifepo4 cell, *J. Power Sources* 210 (2012) 263–275.
- [23] X. Lin, A data selection strategy for real-time estimation of battery parameters, in: 2018 Annual American Control Conference (ACC), IEEE, 2018, pp. 2276–2281.
- [24] X. Lin, Analytic analysis of the data-dependent estimation accuracy of battery equivalent circuit dynamics, *IEEE Contr. Syst. Lett.* 1 (2) (2017) 304–309.
- [25] A.P. Schmidt, M. Bitzer, A.W. Imre, L. Guzzella, Experiment-driven electrochemical modeling and systematic parameterization for a lithium-ion battery cell, *J. Power Sources* 195 (15) (2010) 5071–5080.
- [26] V. Ramadesigan, K. Chen, N.A. Burns, V. Boovaragavan, R.D. Braatz, V. R. Subramanian, Parameter estimation and capacity fade analysis of lithium-ion batteries using reformulated models, *J. Electrochem. Soc.* 158 (9) (2011) A1048–A1054.
- [27] M.J. Rothenberger, D.J. Docimo, M. Ghanaatpishe, H.K. Fathy, Genetic optimization and experimental validation of a test cycle that maximizes parameter identifiability for a li-ion equivalent-circuit battery model, *J. Energy Storage* 4 (2015) 156–166.
- [28] Z. Song, H. Hofmann, X. Lin, X. Han, J. Hou, Parameter identification of lithium-ion battery pack for different applications based on cramer-rao bound analysis and experimental study, *Appl. Energy* 231 (2018) 1307–1318.
- [29] Z. Song, J. Hou, H.F. Hofmann, X. Lin, J. Sun, Parameter identification and maximum power estimation of battery/supercapacitor hybrid energy storage system based on cramer–rao bound analysis, *IEEE Trans. Power Electron.* 34 (5) (2018) 4831–4843.
- [30] S. Park, D. Kato, Z. Gima, R. Klein, S. Moura, Optimal experimental design for parameterization of an electrochemical lithium-ion battery model, *J. Electrochem. Soc.* 165 (7) (2018) A1309–A1323.
- [31] Q. Lai, S. Jangra, H.J. Ahn, G. Kim, W.T. Joe, X. Lin, Analytical sensitivity analysis for battery electrochemical parameters, in: 2019 American Control Conference (ACC), IEEE, 2019, pp. 890–896.
- [32] J.C. Forman, S. Bashash, J.L. Stein, H.K. Fathy, Reduction of an electrochemistry-based li-ion battery model via quasi-linearization and pade approximation, *J. Electrochem. Soc.* 158 (2) (2011) A93–A101.
- [33] S. Moura, Single Particle Model with Electrolyte and Temperature: an Electrochemical Battery Model. <https://github.com/scott-moura/SPMeT> accessed: 2019-08-20.
- [34] S. Alavi, C. Birk, D. Howey, Time-domain fitting of battery electrochemical impedance models, *J. Power Sources* 288 (2015) 345–352.
- [35] J. Song, M.Z. Bazant, Effects of nanoparticle geometry and size distribution on diffusion impedance of battery electrodes, *J. Electrochem. Soc.* 160 (1) (2013) A15–A24.
- [36] K.B. Hatzell, A. Sharma, H.K. Fathy, A survey of long-term health modeling, estimation, and control of lithium-ion batteries: challenges and opportunities, in: 2012 American Control Conference (ACC), IEEE, 2012, pp. 584–591.
- [37] H.K. Khalil, J.W. Grizzle, Nonlinear Systems, vol. 3, Prentice hall, Upper Saddle River, NJ, 2002.
- [38] J. Andersson, reportA General-Purpose Software Framework for Dynamic Optimization PhD thesis, KU Leuven.
- [39] A.C. Hindmarsh, P.N. Brown, K.E. Grant, S.L. Lee, R. Serban, D.E. Shumaker, C. S. Woodward, Sundials: suite of nonlinear and differential/algebraic equation solvers, *ACM Trans. Math Software* 31 (3) (2005) 363–396.
- [40] S. Jangra, A Framework for Lithium-Ion Battery Simulation and Sensitivity Analysis, Master Thesis, University of California, Davis, 2019.
- [41] G. Fan, K. Pan, M. Canova, A comparison of model order reduction techniques for electrochemical characterization of lithium-ion batteries, in: 2015 54th IEEE Conference on Decision and Control (CDC), IEEE, 2015, pp. 3922–3931.
- [42] Q. Lai, H.J. Ahn, G. Kim, W.T. Joe, X. Lin, Optimization of current excitation for identification of battery electrochemical parameters based on analytic sensitivity expression, in: 2020 American Control Conference (ACC), IEEE, 2020.